Ferroelectrics based absorbing layers

Jianping Hao, Véronique Sadaune, Ludovic Burgnies, Didier Lippens

Journal of Applied Physics

Ferroelectrics based absorbing layers

Cite as: J. Appl. Phys. **116**, 043520 (2014); https://doi.org/10.1063/1.4891728
Submitted: 07 July 2014 • Accepted: 19 July 2014 • Published Online: 30 July 2014

Jianping Hao, Véronique Sadaune, Ludovic Burgnies, et al.

AIP Publishing

Ferroelectrics based absorbing layers

Jianping Hao,[1] Véronique Sadaune,[1,2,a)] Ludovic Burgnies,[1,3] and Didier Lippens[1]
[1]*Institut d'Electronique de Micro-électronique et de Nanotechnologie, UMR CNRS 8520, Université des Sciences et Technologies de Lille, avenue Poincaré, BP 60069, 59652, Villeneuve d'Ascq Cedex, France*
[2]*IEMN, Département OAE, Université de Valenciennes et du Hainaut-Cambrésis, UMR CNRS 8520, Le Mont Houy, 59313 Valenciennes Cedex 9, France*
[3]*Université du Littoral Côte d'Opale, 62228 Calais Cedex, France*

(Received 7 July 2014; accepted 19 July 2014; published online 30 July 2014)

We show that ferroelectrics-based periodic structure made of $BaSrTiO_3$ (BST) cubes, arrayed onto a metal plate with a thin dielectric spacer film exhibit a dramatic enhancement of absorbance with value close to unity. The enhancement is found around the Mie magnetic resonance of the Ferroelectrics cubes with the backside metal layer stopping any transmitted waves. It also involves quasi-perfect impedance matching resulting in reflection suppression via simultaneous magnetic and electrical activities. In addition, it was shown numerically the existence of a periodicity optimum, which is explained from surface waves analysis along with trade-off between the resonance damping and the intrinsic loss of ferroelectrics cubes. An experimental verification in a hollow waveguide configuration with a good comparison with full-wave numerical modelling is at last reported by measuring the scattering parameters of single and dual BST cubes schemes pointing out coupling effects for densely packed structures. © *2014 AIP Publishing LLC*.
[http://dx.doi.org/10.1063/1.4891728]

I. INTRODUCTION

Metamaterial–based electromagnetic absorbers are now attracting a huge interest owing notably of the numerous potential applications, which can be foreseen in sensing, wireless telecommunication, electromagnetic compatibility, and stealth and energy harvesting. Also, they can be considered as canonical artificial structures for electromagnetic wave dispersion engineering by taking advantage simultaneously of an electric and magnetic response.[1–3] One of the first proposal for the use of metamaterial technologies aimed at fabricating absorbing layers was published in 2002 by Engheta.[4] The structure consists in Split Ring Resonator (SRR) and wire arrays so that a double electrical and magnetic characteristic response allows suppressing any transmitted and reflected waves simultaneously with thus a quasi-unitary absorbance. For the magnetic response of SRR arrays, a proper polarization of the magnetic field is required by a grazing incidence with respect to the SRR printed circuit board. This requirement about the *H*-field polarization is troublesome from the realization of thin film absorbers. As a consequence, other alternatives have been proposed notably by using two cut wires in close proximity. For such a basic cell, a current loop can be induced by the incident magnetic field under normal excitation. On this concept, one of the first analysis of a planar Perfect Metamaterial Absorbers (PMA) was published in 2008 and this reference being considered as one of the seminal papers in the field of PMA.[5] The basic cell, used in this reference, consists in I-shaped electrical resonators, which exhibit electric and magnetic resonance when there are coupled via a thin dielectric layer.

Owing to coupling effects, the anti-parallel current configuration gives rise to a magnetic response under normal incidence, since these pioneering works many novel patterns have been reported in the literature;[6] such as Cross,[7] patch,[8–10] snowflake,[11,12] spiral to mention a few. Also the absorbers design operating at microwave frequencies was simplified via the use of a backside metal plate as in conventional Salisbury screen[14] or Jaumann layer.[15] By the introduction of novel pattern, higher functionality and better performance have thus been obtained in terms of multiband operation,[13,16–20] lower sensitivity to polarization, and higher robustness with respect to the incidence angle.[13,21–26]

For the latter issue, one of the main difficulties is that intrinsically the response of planar structure is anisotropic with a magnetic response, which results from conduction current. In contrast, the magnetic response in Mie-resonance based metamaterial is intrinsically isotropic owing to bulk displacement current flow.[27–29] Recently, we showed that ferroelectric cubes exhibit isotropic electromagnetic characteristics with a ground Mie-type resonance, which can be attributed to the creation of an artificial magnetic dipole. Also, an electrical polarization can be induced at higher frequencies. Both resonances do not overlap at least for uniform size cube arrays and such a ferroelectrics-based metamaterial can be considered as a single negative medium for each magnetic and electrical resonance frequency bands. However, it was recently reported that ferroelectric particles (spheres/cubes) set onto a ground metal plate exhibit near perfect absorbance.[29] In this reference, it was shown that the ferroelectric inclusions couple to the incident magnetic fields and the metallic ground plane couples to the incident electrical field so that impedance matching to free space can be achieved.

The work reported in the present paper is based on the same principle of surface impedance matching of

[a)]Electronic mail: Veronique.Sadaune@univ-valenciennes.fr

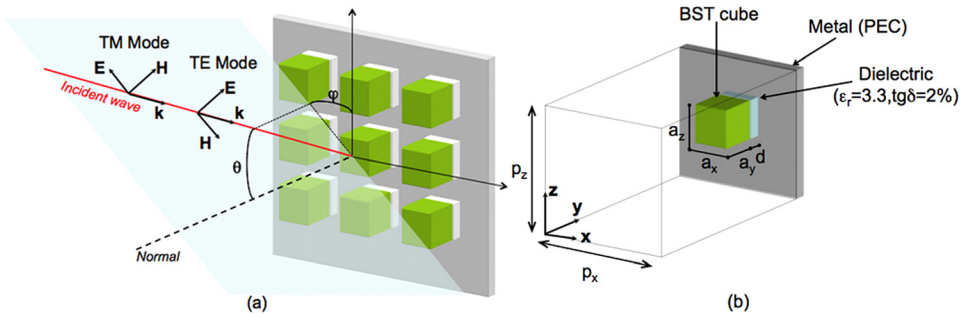

FIG. 1. Schematic of (a) the metamaterial absorber with illustration of the TE and TM polarization modes of the incident wave and the definition of incidence angles: θ and φ (the shaded blue plane represents the plane of incidence) and (b) the basic cell with its characteristic parameters.

ferroelectric cubes arrayed onto a metal ground plane. Beyond the study of absorption properties of elementary ferroelectric scatterers with emphasis on the particle size, special attention was paid here (i) to the integration of a ferroelectric cube shaped-array without or with a spacing layer (ii) coupling and (iii) array effect showing periodicity impact. Also a study is performed on the sensitivity on the incidence angle, which is one of the key properties of electromagnetic absorbers.

Towards these goals, we first retain the basic idea of the combination of the $BaSrTiO_3$ (BST) magnetic resonance, observed in bare (without ground metal) cube arrays[27] and the electrical response due the ground metal plane by assuming a direct interfacing between ferroelectrics and metal or using a low permittivity spacing layer. For the latter, significant frequency shifts ($\Delta f \sim 2$ GHz for an operation at X 8–12 GHz microwave band) were noticed and explained by the modification of boundary conditions with respect to a direct interfacing of BST cube with metal. As a consequence, the final version of a perfect metamaterial absorbers based on ferroelectrics assessed experimentally includes a thin dielectric layer sandwiched between the ferroelectric particles and the backside metal plate.

The paper is organized as follows: Sec. II deals with a numerical study based on a full wave analysis of BST cubes arrayed onto a metal plate without and with a dielectric spacer layer. We mainly computed (i) the complex reflection coefficient (S_{11}) versus frequency and (ii) the dispersion characteristic (angular frequency ω versus complex propagation constant γ). By varying the period of array, it is shown the existence of an optimum, which is explained by the cross-over between propagating surface waves and localized states. Also, some trade-offs are also evidenced for the loss tangent of ferroelectrics. Experimentally in Sec. III, a dramatic enhancement of the absorbance of millimeter size ferroelectric cubes array backed by a copper plate was assessed via Vector Network Analysis of $BaSrTiO_3$ single and dual cubes. For the characterization stage, samples are put in a hollow metal waveguide mimicking thus periodic structures via mirrored images. Concluding remarks and prospects are reported in Sec. IV.

II. NUMERICAL ANALYSIS

A. Basic principle of impedance matching

The basic principle used in this ferroelectric metamaterial absorber to obtain a reflectivity close to 0 is the Mie resonance that provides an efficient mechanism to match the free space impedance at the resonance frequency whereas a metallic ground plane stopped the transmitted wave.

The design of the metamaterial absorber consists of a ferroelectric high permittivity cubes interfaced, in its experimental version, by a thin (0.2 mm) low permittivity ($\varepsilon_r = 3.3$) dielectric layer with a metallic backside plate. These cubes are structured in the transverse directions in square array at a sub-wavelength scale. A schematic of the structure and of the basic cell is shown in Fig. 1. For an incident wave normal to the surface, the electric field is along the z axis and the magnetic field is along the x axis.

The ferroelectric material used for the cubes is BST with a barium concentration of 50% and a MgO doping of 15 wt. %.[30] The cubes have a side length of 1.8 mm. According to our previous studies,[31] the BST material has a complex permittivity of 132(1–0.015i). With such values of permittivity and size, the relevant Mie resonance frequencies are in the X (8–12 GHz) and Ku (12–18 GHz) bands.

The commercial softwares COMSOL Multiphysics and HFSS by Ansys were used to perform the full-wave simulations. For analysis under normal incidence, the basic cell was artificially repeated by using Perfect Electrical Conductor (PEC) and Perfect Magnetic Conductor (PMC) boundary conditions. For the study of incidence sensitivity, Floquet ports and master slave boundaries were used.

As the transmission is suppressed due to the back metallic plate, the absorption is calculated by $A = 1 - |S_{11}|^2$. Fig. 2 shows the absorbance spectrum simulation result

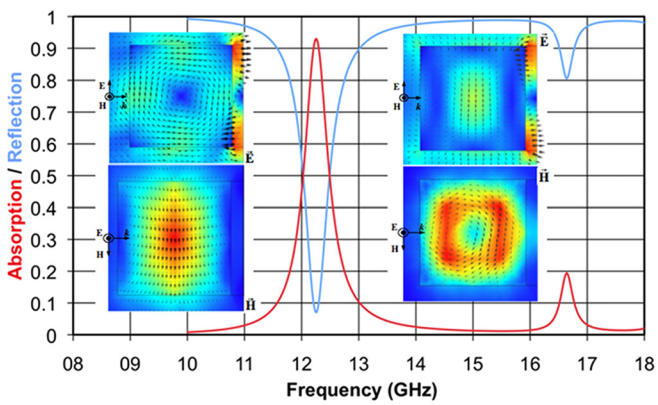

FIG. 2. Reflection and absorption spectra for an array of BST cubes on a 0.2 mm-thick dielectric layer and a back metal plane. In insert, the ***E***- and ***H***-field maps recorded for the two resonance peaks in the zy and xy planes, respectively, at the center of the cubes.

under normal incidence when the cubes are arrayed on the metal plate with a 0.2 mm-thick dielectric spacer layer.

Two absorption peaks are pointed out, in the frequency range of interest, located at 12.25 GHz and 16.64 GHz. The first resonance around 12 GHz is the strongest with an absorbance as high as 92% while the second one, around 16.5 GHz, is much weaker. The ***E***- and ***H***-field maps recorded for these two resonances peaks in the *zy* and *xy* planes (see Fig. 1(b)) respectively at the center of the cubes are plotted in Fig. 2 insert (***E*** in the upper and ***H*** in the lower panels). For the first resonance, a current loop which results from the *displacement* current wrapping around the ***H*** incidence *x* axis can be noticed. It results a magnetic dipole that corresponds to the ground *Mie-type* magnetic resonance. Along the *x* axis, an elongation of the magnetic dipole can be pointed This is the signature of magnetic dipole coupling effect more sensitive for this direction.[32] The second resonance is consistent with an electrical response as assessed by the creation of an electrical dipole along the *z* direction and the ring-shaped in ***H***-field contours. For both resonances, strong electric field confinement can be seen in the spacer layer as a result of the continuity of the displacement vector ***D***. The large difference in the relative permittivity between the ferroelectric layer ($\varepsilon_r \sim 100$) and the spacer layer ($\varepsilon_r \sim 3$) explains this accumulation. Owing to more pronounced absorption effect around 12 GHz, in the following, we will focus our attention around the first Mie magnetic resonance.

B. Geometrical parameters influence

From the geometrical point of view, several parameters are expected to play a major role in the determination of the resonance frequencies. Hereafter special attention will be paid to the influence of two of them involved in coupling phenomena namely the thickness of the dielectric spacer layer and the array periodicity.

1. Influence of the spacer thickness

In this first section, we consider the thickness (d) of the low permittivity spacer between the BST cube array and the backside metallic plane. Let us remind that, from a practical point of view, this spacer simulates the adhesive layer used to maintain the BST cubes in experiment. For the simulation, we assumed a polyimide-type thin layer with a typical complex permittivity of 3.3(1–0.02i). Fig. 3 shows the absorption obtained by varying the thickness d from 0 to 5 mm.

When the cubes are deposited directly onto the metal plate ($d = 0$), it can be noticed a strong down-frequency shifting of around 2 GHz, with respect to finite thickness dielectric responses. For this *zero-d* configuration, it can be shown that the presence of the metal plate directly in contact with BST cubes modifies the current loop in a half circle pattern in the propagation direction. From mirrored images considerations, it results a *virtual* larger size cube, which explains the frequency shift at lower frequencies. In contrast, for finite value of d, only slightly resonance frequency shift can be evidenced.

Regarding the maximum of the absorption, it increases slowly from 92% at 0.1 mm to 99.99% at 1.8 mm and then decreases rapidly. If we analyze the field map for the various

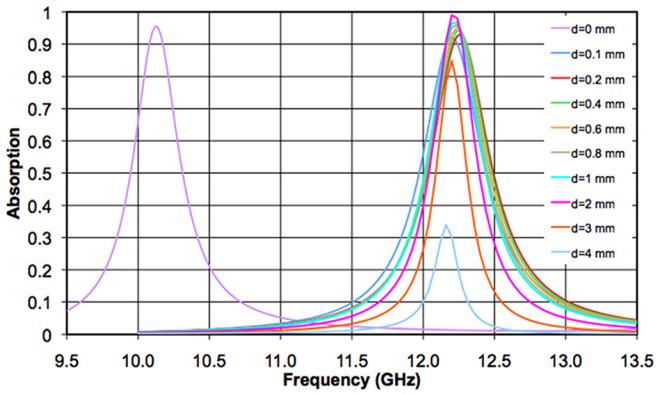

FIG. 3. Influence on the absorption of a dielectric spacer of thickness d, varying from 0 mm to 4 mm, with a complex permittivity equal to 3.3(1-0.02i).

spacer sizes, it was found that the maximum of absorption corresponds to the maximum of the magnetic field into the cubes, which increases slightly up to 1.8 mm for dropping after. In conclusion, the spacer thickness influences the magnetic dipole induced by the displacement currents and when its strength becomes weaker, the absorption becomes more sensitive to the spacer size. Similar behaviors were also been found in SRR-type metamaterial absorber.[33]

Another way to analyze the various mechanisms which are involved in the absorption process around 12 GHz is to consider the first Mie magnetic resonance of the BST inclusions. The second mechanism is interference due to the wave in the BST/spacer layer, totally reflected by the metallic plate and partially reflected/transmitted at the BST cube interface. The spacer acts as an asymmetric Fabry-Perot cavity. The multiple reflections that occur in it can be constructive or destructive at the interface cube/air according to the spacer thickness.[34] At a last comment, let us mention that the use of a thin sticking tape does not degrade the absorption.

2. Influence of the periodicity

For the periodic arrays investigated in the present work, it is expected that the period influences the absorptivity via coupling effects. For illustrating such *array* effects, we thus plotted in Fig. 4 the frequency dependence of the absorbance

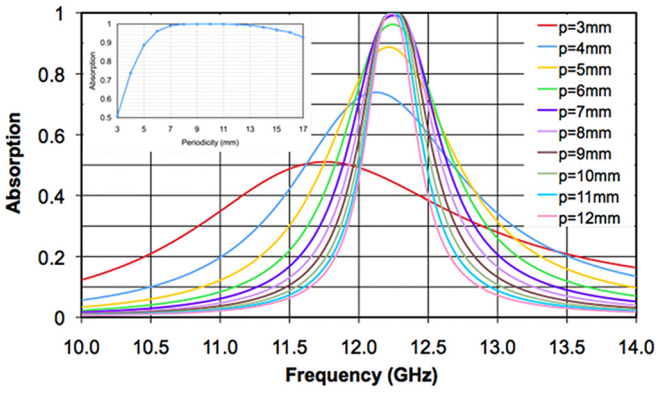

FIG. 4. Influence of the periodicity of the BST array ($p = p_x = p_z$) on the absorption spectra for p varying from 3 mm to 17 mm. Maximum of absorbance versus the period array is plotted in insert.

calculated by varying the period (p) from 3 to 17 mm by 1 mm step.

The results displayed in Fig. 4 show unambiguously that the resonance frequency, the maximum of absorption along with the spectral broadening, characterized by the Full Width at Half Maximum (FWHM) are strongly dependent on periodicity and thus on array effects. For the lowest period of $p = 3$ mm, which corresponds to an interspacing between cubes of 1.2 mm, a significant frequency shift is evidenced numerically with a resonance frequency close to 11.7 GHz instead of 12.3 GHz. This lower frequency shift can be explained the coupling effect between adjacent BST cubes, that we studied in Ref. 32 for bare cubes array. Surprisingly, at first analysis, it can be noticed that the maximum of absorbance is not achieve for the more densely packed structure but for an optimum value $p = 9$ mm. The Inset of Fig. 4 however shows that the period dependence of the absorbance maxima is relatively flat with values close to unity on a relatively broad range of p values.

For a deeper understanding of these array effects, the dispersion characteristic as a function of the in plane $\boldsymbol{k}$ vector ($k_{//}$) were calculated by means of eigenmode solver of HFSS numerical code. The results in terms of eigenfrequencies versus reduced $\boldsymbol{k}$ vector for $p = 6$ mm in the first Brillouin zone are reported Fig. 5. The highly localized states, which correspond to the quasi-flat dispersion branches, were found in agreement with scattering parameters calculations, i.e., around 12 GHz for the magnetic resonance, and around 16 GHz, for the electric one. For each localized states around 12 GHz corresponds one direction (x, y or z) of the magnetic field. Only localized state with $\boldsymbol{H}$ in the y direction is invariant with $k_{//}$ while the slight slope observed at low $k_{//}$ for the two other localized states is the signature of the coupling between BST cubes with $\boldsymbol{H}$ in x or z direction. The waves propagating in the vicinity of the metal layer corrugated via the BST cube array (blue square symbols) show a typical surface wave characteristic. The corresponding dispersion branch is tangent in the lower frequency part of the spectrum to the light cone (plotted in dotted black line). From Fig. 5, it can be noted that surface mode wave couples to one of the highly localized modes as evidenced via the anti-crossing apparent for reduced k value close to $\pi/2$ for $p = 6$ mm.

The direction of the magnetic field selects the localized state coupled with the surface wave. By increasing p, the anti-crossing between localized and delocalized states shifts toward high $k_{//}$ until going out the first Brillouin zone. For short period, the resonance frequencies are less localized at low $k_{//}$, resulting in a higher slope of the localized states in the dispersion characteristics and a broadening of absorption peak. For larger periods, the coupling between elementary cells decreases with, thus, more localized states with a concomitant increase in the resonance quality. Therefore, there exists a tradeoff between the coupling effect between elementary cells at short period and the coupling of extended states to the highly localized states explaining the existence of optimum value in the maxima of absorbance.

C. Material influence

The other parameters influencing the characteristics of the absorber are the complex relative permittivity and notably the loss tangent ($tan\delta$) of the BST cube, which are the primary source of loss in the microwave frequency band considered here. We reproduce here the principal result, which is quite counter-intuitive because it highlights a trade-off on the tangent loss value. Fig. 6 shows the absorption calculated for $tan\delta$ varying from 0.5% to 4%.

From Fig. 6, it can be seen that the absorption presents a maximum at 2.5%. It can be numerically verified (not shown here) that the FWHM of the absorption window increases linearly with $tan\delta$. This can be interpreted in terms of lifetime of the resonant state, which thus varies as the inverse of $tan\delta$. The optimal value in the loss tangent of the dielectric system pointed out in Fig. 6 is a direct consequence of a trade-off between the quality of the resonance, which enhances the overall absorbance (A) around the resonance frequency and the amount of intrinsic loss.

Such a finding demonstrated here for ferroelectric dielectric system is in accordance with the result found in Ref. 35 for plasmonic resonator systems. In this reference, it is shown that the total absorption is achieved provided the wave attenuation via the decay time constant due to

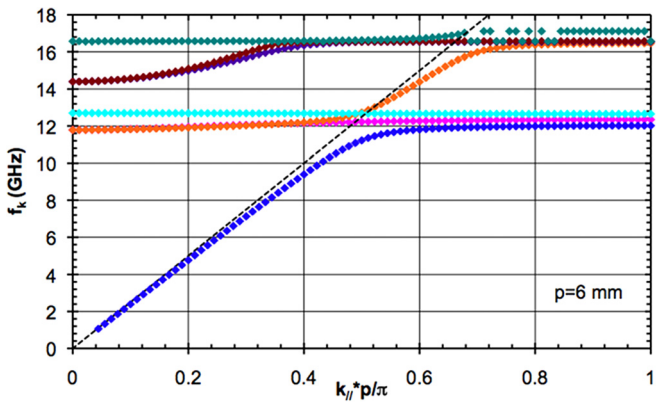

FIG. 5. Dispersion characteristic for $p = 6$ mm. Highly localized eigenstates of the BST magnetic resonator are square in light blue, rose, and orange symbols around the magnetic travelling surface wave (in dark blue square symbol). The black dotted line represented the propagating wave.

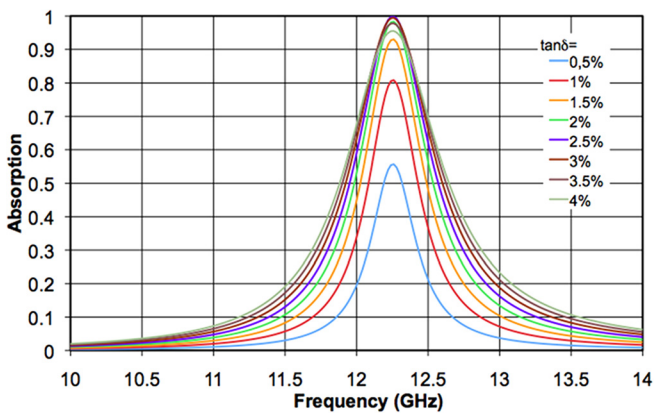

FIG. 6. Absorption spectra for 1.8 mm side BST cube array with a periodicity of 7.2 mm, interfaced with a 0.2 mm-thick dielectric with a metal plate (infinite conductivity) for BST loss tangent varying from 0.5% to 4%.

dielectric loss equals the wave radiation time, which leads to an optimal value for $tan\delta$.

D. Influence of incidence angle

In the present section, we study numerically the isotropy and the polarization sensitivity of the absorber. For this, let us remind that the simulations were performed with HFSS code and use the Floquet ports and master-slave boundaries. As shown in Fig. 1(a), the incident wave is characterized by two angles: θ the incident angle between the wave vector and the normal to the absorber surface and φ the angle between the projection of wave vector on the absorber surface and the z axis. TE and TM modes are also defined on the figure. They correspond respectively to a polarization direction of the electric field or the magnetic field perpendicular to the plane of incidence (represented by a shaded blue plane on Fig. 1(a)), formed by the wave vector and the normal to the absorber surface. The reflection coefficient, as a function of frequency, was calculated taking θ and φ as parameters for both TE and TM modes. On the basis of these calculation, the resonance frequencies and the minima of the reflection coefficients ($S_{11,min}$) have been determined. As a general rule, it was found that magnitude of $S_{11,min}$ was quasi not influenced by the square shaped ferroelectric inclusions. As a consequence, only the dependence of the resonance frequency (f_{res}) and of $S_{11,min}$ as a function of θ will be reported. The results are displayed in Fig. 7 for an incidence angle ranging between 0° and 80° and for TE (light blue dashed line) and TM (red dashed line) modes, respectively.

From Fig. 7(a), it can be noted the resonant frequency has a weak sensitivity to the angle with a maximum variation of 1.5% for TM mode and $\theta = 80°$, hence close to a grazing incidence. In addition, it can be seen TE and TM modes show opposite variations with a more pronounced frequency shift for transverse magnetic mode.

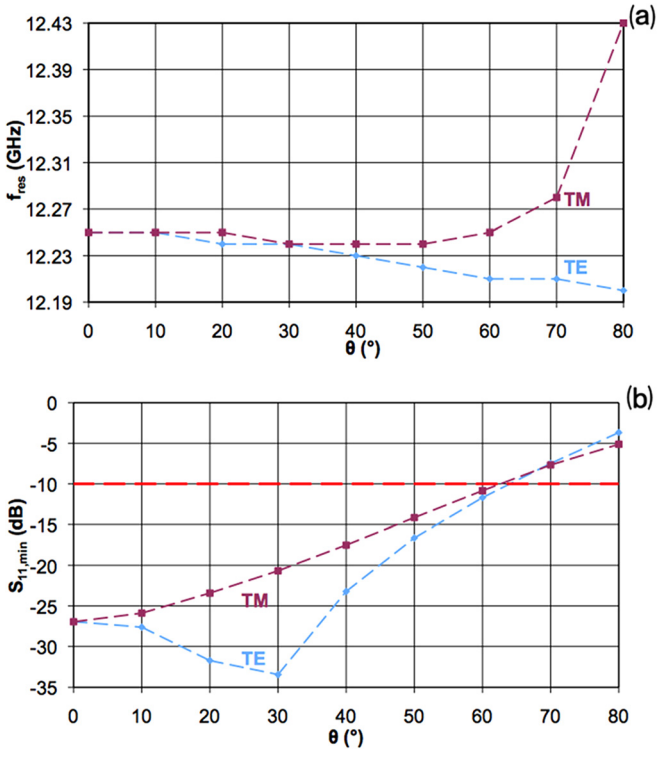

FIG. 7. Resonance frequency dependence (a) and reflection coefficient dependence (b) as a function of θ for TE and TM polarizations.

The weak sensitivity of the resonance frequency to the incidence angle can be expected by reminding that absorption takes place around the magnetic Mie resonance frequency. On this basis, intrinsically isotropic properties are achieved owing to the displacement current loop responsible for magnetic induction. Under these conditions, one can expect slight variation in the relevant dimensions involved in the resonance process. With respect to the magnitude of $S_{11,min}$ reported in Fig. 7(b), its value increases monotonously with θ for the TM polarization. For an incidence angle up to $\pm 60°$, the absorption is greater than 90%. For the TE mode, it can be observed a minimum in the reflection coefficient for $\theta = 26°$.

For TM mode, the increase of the resonance frequency can be understood from a $k_{//}$ increases with θ, which gives a slight higher resonance frequency according to the dispersion diagram. For this polarization condition, the incident magnetic field is always parallel to BST cube array. Also, qualitatively, when θ increases, the transverse component of the $\boldsymbol{k}$ vector increases with thus a lower ratio between the parallel wavelength and the cube size. For TE polarization, the magnetic Mie resonances can be induced by the two components of the magnetic field ($H_{\perp}$ and $H_{//}$, respectively). Therefore, the incident wave interacts with the cube via the two $\boldsymbol{H}$ components with thus a lower reflectivity for the TE mode with respect to the TM one. The result that the reflection coefficient shows a minimum could be explained by the relative importance of the absorption mechanisms via the transverse and perpendicular $\boldsymbol{H}$ components, respectively.

III. EXPERIMENTAL VERIFICATION

To satisfy the energy conservation principle which has to be verified for absorbance calculation, we use a hollow waveguide configuration and hence a close system to make easier the energy balance. In practice, the experimental assessment was performed in a X-band and Ku-band rectangular waveguides. Let us remind that in that case, the incident wave distribution differs from the one in free space with a TE_{10} dominant mode in the frequency band of interest. This restriction in mind, we focus our attention about the coupling effects illustrated in the previous sections, here for dimers that offers a most simple test-bed for assessing coupling effects. Therefore, the experiment was conducted with two BST cubes in close proximity on a 2 mm-thick aluminum plate. The separation distance between the two cubes is given between their centers either in the magnetic field direction (PH) or in the electric field direction (PE) as depicted in Fig. 8. At last, let us mention that post-experiment simulations were conducted for a hollow waveguide configuration and hence PEC boundary conditions mimicking the metal side walls.

In Figs. 9(a) and 9(b), the simulated and experimental results are compared when PE was increased from 2 mm to 7 mm. While in Figs. 10(a) and 10(b), the simulated and

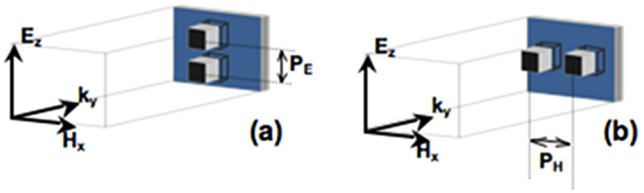

FIG. 8. Schematic of the hollow metal waveguide configuration for assessing the coupling effect.

experimental results were plotted for *PH* ranging from 3 mm to 11 mm.

In both cases, there is an excellent agreement between modeling and experiment for the absorbance peaks and the Mie magnetic resonance frequencies. With respect to the frequency shift induced by coupling, the fit is also good with, however, slight differences in the resonance frequency shift owing to the inaccuracy in the BST cube interspacing. Compared with the result calculated for periodic boundary conditions (Fig. 2), an overall satisfactory agreement can be also noticed.

The influence of *PE* is weak either on the resonance frequency or on the absorption level. On the field maps, shown is insert of Fig. 9 for $PE = 2$ mm and 4 mm, respectively. One can note that the EM-field is always confines in each cube, whatever the distance. In connection with the influence of *PH*, Fig. 10 shows the peak frequency decreases of 760 MHz for $\Delta PH = 9$ mm. This variation is due to the strong coupling effect between the two cubes for this configuration.[36]

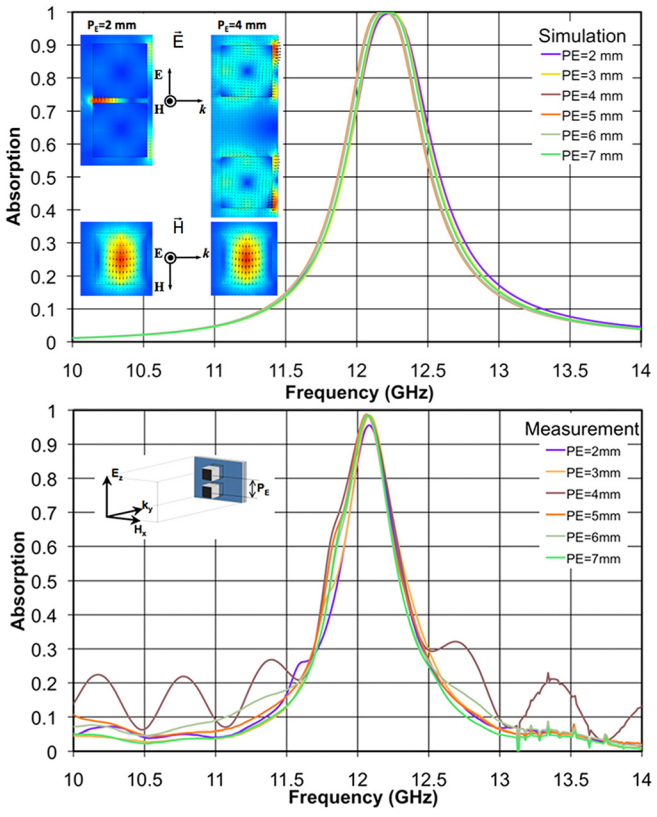

FIG. 9. Simulated and experimental absorption spectra for BST cubes dimer when varying *PE*.

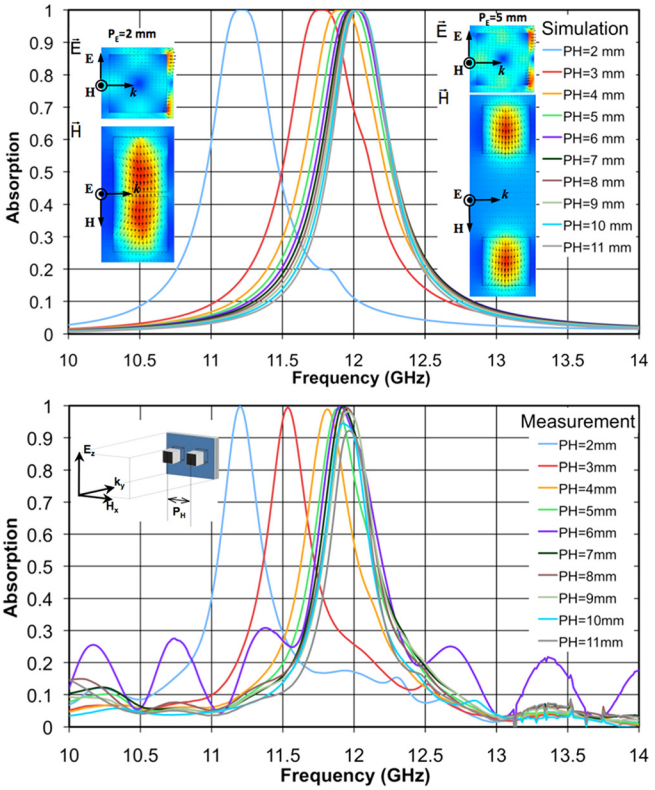

FIG. 10. Simulated and experimental absorption spectra for BST cubes dimer when varying *PH*.

If we have a look to the field maps, reported in insert of the Fig. 10, it can be noted the coupling between longitudinally induced magnetic dipoles increases when *PH* decreases. For small *PH*, everything happens as if the magnetic field was confined in a twin cube inducing a lowering of the resonance frequency. When *PH* increases, the coupling diminishes as the absorption. Experimentally, a maximum of absorption of 99.9% was obtained. The result reported above for a waveguide configuration illustrates the coupling between two ferroelectric cubes. It is believed they also give an indirect assessment of the periodicity effect for a cube inter-distance of 11 mm. As the lateral dimensions of a X-band rectangular waveguide is 22.86 mm by 11.16 mm, this means that when the cube inter-distance is set to 11 mm, the sample under test can be compared with a periodic media with $p = 11$ mm. For this value, it was shown numerically that the peak absorbance is close to one (Fig. 4) in agreement with the experiment reported in Fig. 10(b).

IV. CONCLUSION AND PROSPECTS

By taking advantage of the Mie resonance concept in high permittivity dielectric inclusion, we showed, numerically and experimentally, the enhancement of the absorption of a BST cube array interfaced by a thin low permittivity dielectric layer with a metallic plane. Targeting absorbance magnitude close to unity, we demonstrated the existence of optimal values for the spacer thickness and the array period, which were not expected in a first analysis focused on the basic cell. In addition, the isotropy of the absorber and its sensitivity to the wave polarization has been assessed. From a

practical point of view, we found an absorbance greater than 90% for an angle of incidence up to ± 60° and a slight difference between the TE and TM mode due to the presence of the metallic plane. An experimental demonstration of the basic principle has been conducted and absorption up to 99% has been measured. The next step will be to broaden the absorbance bandwidth without reducing the absorbance via thin film technology and multi-scaled pattern.

ACKNOWLEDGMENTS

The authors would like to thank the University of Tsinghua (Professor Zhou's group) for the fabrication of the BST cubes. Jianping Hao thanks the Chinese Government for her Ph.D. fellowship.

[1]C. Caloz, "Metamaterial dispersion engineering concepts and applications," Proc. IEEE **99**(10), 1711–1719 (2011).
[2]G. Sisó, M. Gil, F. Aznar, J. Bonache, and F. Martín, "Dispersion engineering with resonant-type metamaterial transmission lines," IEEE Laser Photon. Rev. **3**, 12–29 (2009).
[3]Q. Feng, M. Pu, C. Hu, and X. Luo, "Engineering the dispersion of metamaterial surface for broadband infrared absorption," Opt. Lett. **37**, 2133–2135 (2012).
[4]N. Engheta, "Thin absorbing screens using metamaterial surfaces," IEEE Antennas Propag. Soc. Int. Symp. **2**, 392–395 (2002).
[5]N. I. Landy, S. Sajuyigbe, J. J. Mock, D. R. Smith, and W. J. Padilla, "Perfect metamaterial absorber," Phys. Rev. Lett. **100**, 207402 (2008).
[6]C. M. Watts, X. Liu, and W. J. Padilla, "Metamaterial electromagnetic wave absorbers," Adv. Mater. **24**, OP98–OP120 (2012).
[7]N. I. Landy, C. M. Bingham, T. Tyler, N. Jokerst, D. R. Smith, and W. J. Padilla, "Design, theory and measurement of a polarization insensitive absorber for terahertz imaging," Phys. Rev. B **79**, 125104 (2009).
[8]J. Hao, J. Wang, X. Liu, W. J. Padilla, L. Zhou, and M. Qiu, "High performance optical absorber based on a plasmonic metamaterial," Appl. Phys. Lett. **96**, 251104 (2010).
[9]C. Wu and G. Shvets, "Design of metamaterial surfaces with broadband absorbance," Opt. Lett. **37**, 308 (2012).
[10]B. Zhang, J. Hendrickson, and J. Guo, "Multi-spectral near perfect metamaterial absorbers using spatially multiplexed plasmon resonance metal square structures," J. Opt. Soc. Am. B **30**, 656 (2013).
[11]Y. Huang, Y. Tian, G. Wen, and W. Zhu, "Experimental study of absorption band controllable planar metamaterial absorber using asymmetrical snowflake-shaped configuration," J. Opt. **15**, 055104 (2013).
[12]W. Zhu and X. Zhao, "Metamaterial absorber with dendritic cells at infrared frequencies," J. Opt. Soc. Am. B **26**, 2382 (2009).
[13]X. Huang, H. Yang, S. Yu, J. Wang, M. Li, and Q. Ye, "Triple-band polarization-insensitive wide angle ultra-thin planar spiral metamaterial absorber," J. Appl. Phys. **113**, 213516 (2013).
[14]W. W. Salisbury, "Absorbent body for electromagnetic waves," US Patent No. 2599944 (1952).
[15]B. A. Munk, P. Munk, and J. Pryor, "On designing Jaumann and circuit analog absorbers (CA absorbers) for oblique angle of incidence," IEEE Trans. Antennas Propagation **55**, 186 (2007).
[16]M. P. Hokmabadi, D. S. Wilbert, P. Kung, and S. M. Kim, "Terahertz metamaterial absorbers," Terahertz Sci. Technol. **6**, 40 (2013).
[17]Z. H. Jiang, S. Yun, F. Toor, D. H. Werner, and T. S. Mayer, "Conformal dual-band near-perfectly absorbing mid-infrared metamaterial coating," ACS Nano. **5**, 4641 (2011).
[18]J. Zhong, Y. Huang, G. Wen, H. Sun, P. Wang, and O. Gordon, "Single-/dual-band metamaterial absorber based on cross-circular-loop resonator with shorted stubs," Appl. Phys. A **108**, 329 (2012).
[19]F. Ding, Y. Cui, X. Ge, Y. Jin, and S. He, "Ultra-broadband microwave metamaterial absorber," Appl. Phys. Lett. **100**, 103506 (2012).
[20]J. Sun, L. Liu, G. Dong, and J. Zhou, "An extremely broad band metamaterial absorber based on destructive interference," Opt. Exp. **19**, 21155 (2011).
[21]B. Zhu, Z. Wang, C. Huang, Y. Feng, J. Zhao, and T. Jian, "Polarization insensitive metamaterial absorber with wide incident angle," PIER **101**, 231 (2010).
[22]Bi. Wang, T. Koschny, and C. M. Soukoulis, "Wide-angle and polarization-independent chiral metamaterial absorber," Phys. Rev. B **80**, 033108 (2009).
[23]Q. Cheng, T. Jun Cui, W. Xiang Jiang, and B. Geng Cai, "An omnidirectional electromagnetic absorber made of metamaterials," New J. Phys. **12**, 063006 (2010).
[24]S. Chen, H. Cheng, H. Yang, J. Li, X. Duan, C. Gu, and J. Tian, "Polarization insensitive and omnidirectional broadband near perfect planar metamaterial absorber in the near infrared regime," Appl. Phys. Lett. **99**, 253104 (2011).
[25]P. Bouchon, C. Koechlin, F. Pardo, R. Haïdir, and J.-L. Pelouard, "Wideband omnidirectional infrared absorber with a patchwork of plasmonic nanoantennas," Opt. Lett. **37**, 1038 (2012).
[26]Y. Qian Ye, Y. Jin, and S. He, "Omnidirectional, polarization-insensitive and broadband thin absorber in the terahertz regime," J. Opt. Soc. Am. **27**, 498 (2010).
[27]Q. Zhao, J. Zhou, F. Zhang, and D. Lippens, "Mie resonance-based dielectric metamaterials," Mater. Today **12**, 60 (2009).
[28]F. Zhang, Q. Zhao, L. Kang, J. Zhou, and D. Lippens, "Experimental verification of isotropic and polarization properties of high permittivity-based metamaterial," Phys. Rev. B **80**, 195119 (2009).
[29]X. Liu, Q. Zhao, C. Lan, and J. Zhou, "Isotropic Mie Resonance-based metamaterial perfect absorber," Appl. Phys. Lett. **103**, 031910 (2013).
[30]Q. Zhao, B. Du, L. Kang, H. Zhao, Q. Xie, B. Li, J. Zhou, L. Li, and Y. Meng, "Tunable negative permeability in an isotropic dielectric composite," Appl. Phys. Lett. **92**, 051106 (2008).
[31]J. Hao, V. Sadaune, L. Burgnies, E. Lheurette, and D. Lippens, "Ferroelectric metamaterial perfect absorber," in Proc. 7th International Congress on Advanced Electromagnetic Materials in Microwaves and Optics, Metamaterial 2013, Bordeaux, France, September 2013.
[32]F. Zhang, L. Kang, Q. Zhao, J. Zhou, and D. Lippens, "Magnetic and electric coupling effects of dielectric metamaterial," New. J. Phys. **14**, 033031 (2012).
[33]M.-h. Li, S.-y. Liu, L.-y. Guo, H. Lin, H.-l. Yang, and B.-x. Xiao, "Influence of the dielectric-spacer thickness on the dual-band metamaterial absorber," Opt. Commun. **295**, 262 (2013).
[34]H.-T. Chen, "Interference theory of metamaterial perfect absorbers," Opt. Express **20**, 7165 (2012).
[35]A. Sellier, T. V. Teperik, and A. de Lustrac, "Resonant circuit model for efficient metamaterial absorber," Opt. Express **21**, A997 (2013).
[36]F. Zhang, V. Sadaune, L. Kang, Q. Zhao, J. Zhou, and D. Lippens, "Coupling effect for dielectric metamaterial dimer," PIER **132**, 587 (2012).